Tidal influence on carbon dioxide and methane fluxes from tree stems and soils in mangrove forests

Zhao-Jun Yong[1], Wei-Jen Lin[1,2], Chiao-Wen Lin[2], Hsing-Juh Lin[1*]
[1]Department of Life Sciences and Innovation and Development Center of Sustainable Agriculture, National Chung Hsing University, Taichung 40227, Taiwan
[2]Department of Marine Environment and Engineering and The Center for Water Resources Studies, National Sun Yat-sen University, Kaohsiung 80424, Taiwan
Correspondence to: Hsing-Juh Lin (hjlin@dragon.nchu.edu.tw)

Abstract. Mangroves are critical blue carbon ecosystems. Measurements of methane (CH_4) emissions from mangrove tree stems have the potential to reduce the uncertainty in the capacity of carbon sequestration. This study is the first to simultaneously measure the CH_4 fluxes from both stems and soils throughout tidal cycles. We quantified carbon dioxide (CO_2) and CH_4 fluxes from mangrove tree stems of *Avicennia marina* and *Kandelia obovata* during tidal cycles, which have distinct root structures. The mangrove tree stems served as both net CO_2 and CH_4 sources. Compared to those of the soils, the mangrove tree stems exhibited remarkedly lower CH_4 fluxes, but no difference in CO_2 fluxes. ~~*A. marina* (with pneumatophores) exhibited significantly higher CO_2 and CH_4 fluxes than *K. obovata*.~~ The stems of *A. marina* exhibited an increasing trend in the CO_2 flux from low to high tides. On the other hand, ~~while the~~ CH_4 flux showed high temporal variability, with the ~~tree~~ stems of *A. marina* ~~this species~~ functioning as a CH_4 sink before tidal inundation and becoming a source ~~during low tides~~ after ebbing. In contrast, the stems of *K. obovata* showed no consistent pattern of the CO_2 or CH_4 flux. Based on our findings, ~~sampling only during low tides might overestimate the stem CO_2 and CH_4 fluxes on a diurnal scale.~~ ~~t~~The stem ~~CO_2 and~~ CH_4 fluxes of *A. marina* could ~~be~~ vary by up to ~~55% and~~ 1200~~194~~% ~~less~~ when considering tidal influence, compared~~as opposed~~ to ignoring tidal influence. Therefore, sampling only during low tides might under~~over~~estimate the stem CO_2 and CH_4 fluxes on a diurnal scale. ~~Despite the limitations in the experimental design, .~~ ~~t~~This study highlights ~~species distinctness in the greenhouse gas (GHG) fluxes and~~ the necessity of considering tidal influence when quantifying GHG fluxes from mangrove tree stems. Further research is needed to explore the underlying mechanisms driving the observed flux variations and improve ~~our~~the understanding of GHG dynamics in mangrove ecosystems.

1 Introduction

Global methane (CH_4) emissions have reached a record high level (Saunois et al., 2020). Currently, there are two primary methods utilized for assessing global CH_4 emissions: the bottom-up method and the top-down method. The bottom-up method relies on compiling data from greenhouse gas (GHG) inventories and biogeochemical models to infer the sources of emissions. On the other hand, the top-down method involves measuring atmospheric CH_4 concentrations and utilizing transport models to infer the sources of emissions in order to estimate and assess CH_4 emissions on a global scale. CH_4 emissions estimated by

已設定格式: 英文 (美國)
已設定格式: 字型: 斜體
已設定格式: 下標

the bottom-up method are significantly higher than those estimated by the top-down method, indicating a high degree of uncertainty and suggesting that some sources may be overlooked or not well understood (Jackson et al., 2020). CH_4 generated in wetlands can be released into the atmosphere not only through diffusion, ~~bubbles~~ebullition, and transport mediated by herbaceous plants but also through the stems of woody plants (Gauci et al., 2010; Terazawa et al., 2007). Pangala et al. (2017) demonstrated that the difference between the top-down and bottom-up estimates of CH_4 emissions could be accounted for by the upscaled CH_4 flux from tree stems, emphasizing the necessity of considering this pathway in carbon budgets (Carmichael et al., 2014). Furthermore, forest wetlands account for approximately 60% of the global wetland area, highlighting the potential contribution of woody stems to the global GHG emissions (Barba et al., 2019a; Covey and Megonigal, 2019). While carbon dioxide (CO_2) exchange at the stem–atmosphere interface has been examined (Teskey et al., 2008), little is known regarding the sources and mechanisms of CH_4 emissions originating from tree stems relative to those originating from other pathways. CH_4 emitted by tree stems may originate from microorganisms or cryptogams within the stem bark (Jeffrey et al., 2021; Lenhart et al., 2015) or from the soil, where it is produced and enters the roots before being transported in either liquid or gaseous form through xylem or aerenchyma tissue (Kutschera et al., 2016; Vroom et al., 2022).

GHG emissions from tree stems exhibit temporal and spatial variations with different influencing mechanisms in various studies: i) the tree stem GHG flux tends to be higher during the growing season and lower during the dormant season, but there may also be no significant differences among seasons (Barba et al., 2019b; Köhn et al., 2021; Pangala et al., 2015; Pitz et al., 2018; Wang et al., 2016; Zhang et al., 2022); ii) significant variations in the GHG fluxes from tree stems have been observed at different heights above ground level, with a decreasing trend along the tree ~~trunk~~ stem height (Moldaschl et al., 2021; Pangala et al., 2013, 2014, 2015; Sjögersten et al., 2020), although some studies have not reported this phenomenon (Machacova et al., 2021; Wang et al., 2016); iii) the tree stem GHG emissions may be regulated by various environmental factors such as temperature, moisture, and redox potential (Barba et al., 2019b; Gao et al., 2021; Jeffrey et al., 2019; Pitz et al., 2018; Schindler et al., 2020, 2021; Sjögersten et al., 2020; Terazawa et al., 2015), which can be affected by the fluctuations of water table height ~~fluctuations~~ due to seasonal changes and hydrological processes (Jeffrey et al., 2023; Peacock et al., 2024; Terazawa et al., 2021); iv) tree physiological factors such as lenticel density, wood density, ~~and~~ water content, and stem bark structure may also influence the GHG fluxes originating from tree stems (Jeffrey et al., 2024; Pangala et al., 2013, 2014, 2015; Wang et al., 2016; Zhang et al., 2022).

However, most related studies have focused on freshwater wetlands and upland forests, while relatively limited research has focused on mangrove forests. Jeffrey et al. (2019) reported that dead mangrove trees may contribute approximately 26% to the CH_4 emissions in mangrove ecosystems. However, He et al. (2019) reported inconsistent results, revealing a relatively small contribution from tree stems. The contribution of mangrove tree stems to the total GHG flux in ecosystems is generally less than that in soil (Gao et al., 2021; He et al., 2019; Jeffrey et al., 2019) but still has the potential to exceed 50% (Zhang et al., 2022). Additionally, the GHG fluxes from mangrove tree stems vary among tree species (Zhang et al., 2022) and may even differ within a single tree species (Gao et al., 2021), highlighting the uncertainty in the GHG emissions from mangrove tree stems and emphasizing the need for further investigation.

Mangroves are primarily distributed in tropical and subtropical coastal regions and are regarded as critical ecosystems with a high capacity for sequestering blue carbon (Li et al., 2018; Duarte de Paula Costa and Macreadie, 2022). The anaerobic conditions resulting from tidal inundation, along with the abundant organic matter, turn mangrove soil into a ~~natural~~ ~~substantial~~ source of CH_4 emissions (Lin et al., 2020). This, in turn, impacts their role in mitigating global warming. Moreover, several studies have demonstrated the influence of tides on the emission of GHGs in coastal wetlands ~~(Lin et al., 2023)~~. In both seagrass meadows and tidal marshes, the CH_4 flux tends to peak ~~before the rising tide~~ when tidal water reaches the sampling site (Bahlmann et al., 2015; Capooci and Vargas, 2022). The sudden release of CH_4 can occur through physical force under the influence of tidal movement (Li et al., 2021), resulting in the advective exchange of groundwater or soil pore water with the overlying surface water (Billerbeck et al., 2006; Rosentreter et al., 2018). CH_4 emissions during tidal inundation may be higher if tidal water contains high concentrations of dissolved CH_4 ~~and nitrous oxide (N_2O)~~, which can increase the emissions of CH_4 ~~and N_2O~~ through diffusion due to the concentration gradient (Sturm et al., 2017; Tong et al., 2013). Yamamoto et al. (2009) reported a positive correlation between the water table and GHG fluxes in the flooded littoral zone with vegetation, suggesting that the water pressure rather than gas diffusion primarily affects the emissions of CO_2 and CH_4 across the water–atmosphere interface by ejecting gases from pore spaces. This finding is contrary to previous results in which lower CH_4 fluxes were observed during high tide, which may be caused by the higher water pressure limiting CH_4 diffusion in soil pore spaces filled with water and plant-mediated transport (Tong et al., 2010; Tong et al., 2013). Additionally, CH_4 may be oxidized during diffusion in water (Tong et al., 2013). Furthermore, if the dissolved oxygen concentration, sulfate concentration, and salinity are high in tidewater, this may inhibit CH_4 production and/or promote CH_4 oxidation (Huang et al., 2019), resulting in lower CH_4 emissions during high tides. The variation in the CH_4 flux across the water–atmosphere interface during tidal inundation could be driven by current or wind-induced turbulence (Sturm et al., 2017). CH_4 emissions even exhibited different trends during spring and neap tides (Huang et al., 2019; Tong et al., 2013). However, to our knowledge, there is only one study on the GHG fluxes from mangrove tree stems during tidal cycles (Epron et al., 2023).

This study aimed to quantify the CO_2 and CH_4 emissions from the tree stems of *K. obovata* and *A. mariana*, which are the dominant mangrove species with distinct root structures distributed on the northern and southern coasts of Taiwan, respectively. We investigated the temporal variations in the stem GHG fluxes during tidal cycles and assessed the influence of tides on the upscaled flux. We also simultaneously measured the GHG emissions from mangrove soil, even during tidal inundation, to compare the temporal dynamics of GHG fluxes between the tree stems and soil. We hypothesized that the GHG fluxes from mangrove tree stems and soil exhibit synchronized temporal and species variation during the tidal cycle and that the tidal cycle may exert a significant impact on GHG emissions on a larger scale.

2 Materials and Methods

2.1 Site description

This study focused on the mangroves at four sites along the western coast of Taiwan (Fig. 1). The dominant mangrove species in Wazihwei (K-WZW; 25°10′N, 121°25′E) and Xinfeng (K-XF; 24°55′N, 120°58′E) is *Kandelia obovata*, while *Avicennia marina* is the dominant species in Fangyuan (A-FY; 23°56′N, 120°19′E) and Beimen (A-BM; 23°17′N, 120°6′E). K-WZW and K-XF are situated in northern Taiwan, a subtropical region, with average annual precipitation values of 2023 and 1537 mm, respectively. A-FY and A-BM are located in southern Taiwan, a tropical region, with average annual precipitation values of 1162 and 1603 mm, respectively. A ~~-FY~~BM has the largest forest area (~~68~~75.~~73~~ ha), while ~~A~~K-~~BM~~XF ~~hw~~as the smallest (~~58~~.~~48~~12 ha). Mean tree height across all sites ranged from 1.8 to 5.1 m, and ~~mean~~ tree density and ~~mean~~ diameter at breast height (DBH) avera~~ran~~ged ~~from~~ 0.6 ~~to~~ 2.4 tree m^{-2}~~,~~ and 5.6 ~~to~~ 10.5 cm, respectively (Table 1). The tides were semidiurnal ~~in~~ at all sites. The soil texture at all sites is silt, with an average grain size of 0.046 mm. During the summer ~~season~~ (the study period), the average air temperature was 28.4 °C for *K. obovata* and 29.4 °C for *A. marina* (Lin et al., 2023). The sampling campaign was conducted ~~during the summer season,~~ from 1 June 2022 to 29 July 2022, with each site sampled for 3 days ~~throughout the campaign, all~~ during the spring tide (Table 1). This period was chosen mainly because there is a higher GHG flux in summer compared to~~than during the~~ other seasons, as indicated by preliminary studies conducted at the same site~~s~~ (Lin et al., 2020).

已設定格式: 字型: (英文)Times New Roman

已設定格式: 上標

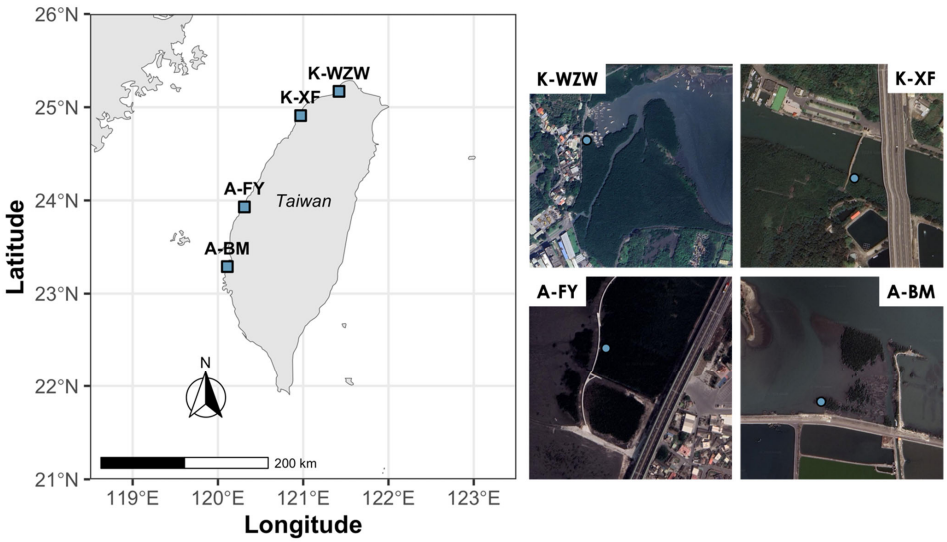
26°N
25°N
24°N
23°N
22°N
21°N
Latitude
119°E
120°E
121°E
122°E
123°E
Longitude
K-WZW
K-XF
A-FY
Taiwan
A-BM
N
200 km
K-WZW
K-XF
A-FY
A-BM

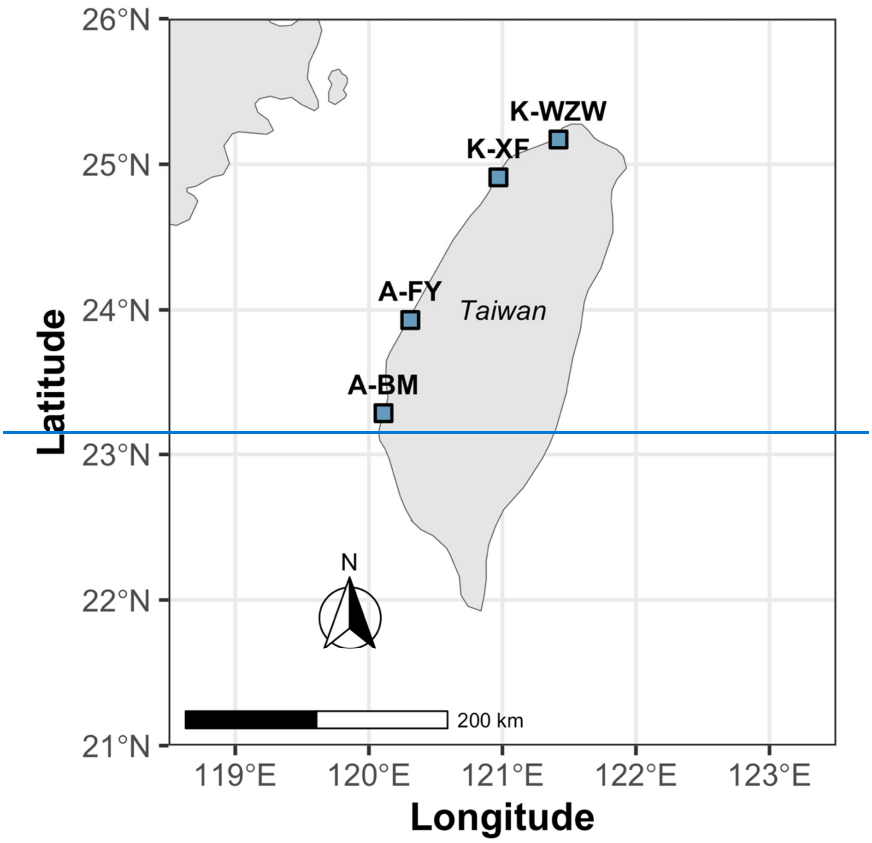

Figure 1. Sample sites along the western coast of Taiwan. The blue dots represent the locations of sampling trees~~the sample tree at each site~~. K-WZW: Wazihwei; K-XF: Xinfeng; A-FY: Fangyuan; A-BM: Beimen. The dominant mangrove species in K-WZW and K-XF is *Kandelia obovata*, while *Avicennia marina* is the dominant species in A-FY and A-BM. M~~(m~~ap sources: Natural Earth (left) and Google Earth (right)).

2.2 Flux measurements and calculation

At each sampling site, a mangrove tree was selected for the tree stem CO_2 and CH_4 flux measurements at approximately 110 cm above the ground. The specific height was chosen considering the potential maximum tidal height due to the consideration of the potential highest tidal height, which may reach up to 80 cm above the ground (Table 1). Due to the differences in the stem morphology, two distinct stem chambers—a semirigid chamber and a cylindrical chamber—were used in this study to measure the GHG emissions of *K. obovata* and *A. marina*, respectively (Fig. S1).

The semirigid chamber was modified from Siegenthaler et al. (2016) and was constructed from transparent recycled polyethylene terephthalate (rPET) bottles. A plastic sheet measuring 14 cm in length and 11 cm in width was cut from a bottle, and 2 cm wide and 1.5 cm thick chloroprene (CR) foam tape was attached around the edges and center of the plastic sheet, with two holes drilled and fitted with adapters for connecting the tubing, resulting in a chamber with a 16 cm^2 surface area and a 0.2 L volume.. The chamber was installed on the tree stem with a strap prior to the measurement and subsequently removed. The second cylindrical chamber was constructed from a 0.2 L white polypropylene (PP) bottle, a 16 cm^2 square was cut from the lid, and two small holes were drilled at the bottom of the bottle; these holes were fitted with adapters to connect the tubing. The lid was fixed to the stem and sealed with silicone prior to the measurement. After eachthe measurement, the chamber was removed, but the lid remained on the trunk (Fig. S1).

Two soil surfaces within 2 m of the sampled tree were selected for soil and water–atmosphere interface CH_4 and CO_2 flux measurements during the tidal cycle using a static chamber (Lee et al., 2011) and the floating chamber method (Lin et al., 2024), respectively. The soil chamber comprised a semicircular transparent polymethyl methacrylate (PMMA) cover (diameter of 30 cm) and a stainless steel ring (height of 16 cm and diameter of 30 cm) with an adapter on the cover for connecting the tubing. The ring was pressed into the soil before placing the cover over it, and a long-tailed clip was used to secure and cover the steel ring tightly to achieve an airtight seal (Fig. S1). During high tide, if the water level exceeded the height of the soil chamber (16 cm), the floating chamber was used (Fig. S1).

In this study, a portable gas analyzer (LI-7810, LI-COR Bioscience, NE, USA) was used to simultaneously measure CO_2 and CH_4 fluxes. The chamber was connected to the analyzer through tubing, and the gas inside the chamber was drawn into the analyzer with a pump, with each measurement lasting approximately five and seven minutes for the stem and soil, respectively. During the tidal cycle, tree stems and soil GHG fluxes were measured consistently. After each measurement was completed, the airtight sealed chamber was opened for approximately 3 minutes to allow the GHG concentration within the chamber to stabilizeAfter each measurement was completed, the airtight sealed chamber was opened up, with for approximately 3 minutes intervals, to allow the GHG concentration within the chamber to stabilize. The water level adjacent to the sampled trees was measured by a tape measure fixed on a PVC pipe (Fig. S1), simultaneously at the beginning of the flux measurement. To minimize soil disturbance, the researcher remained stationary inat one location during the sampling campaign, avoiding walking around. Sampling was mainly conducted during daylight hours. Soil GHG flux data were mainly derived from Lin et al. (unpublished2024). The GHG flux (F) was calculated using the following equation:

$$F = (S \times V \times c)/(RT \times A) \quad (1)$$

Wwhere sS is based on the slope obtained from the linear regression of GHG concentration changes over time (ppb CH_4 s^{-1}; ppm CO_2 s^{-1}), V is the chamber volume (L), c is the conversion factor from seconds to hours, R is the ideal gas constant (0.082 L atm K^{-1} mol^{-1}), T is the air temperature inside the chamber (K), and A is the surface area of the chamber (m^2). a more detailed description of the GHG flux calculation process can be found in Lin et al. (2020) and Lin et al. (2021). If the R^2 of the linear regression was >< 0.7, the GHG flux was removed from the further statistical analysis. The surface area and volume of the semirigid chamber were calculated as described by Siegenthaler et al. (2016).

Different upscaling methods were applied to the tree stem GHG fluxes. First, the average fluxes during low and high tides were multiplied by the non-inundation time and inundation time length in hours, respectively. These values were then summed to calculate the daily fluxes, accounting for the tidal influence, which is denoted as "$F_{BothTide}$". Since sampling in mangrove forests was mostly conducted during low tide, the average fluxes during low tides were multiplied by 24 hours to scale up to daily fluxes, denoted as "$F_{LowTide}$", to compare with the fluxes accounted for tidal influence. The equations are shown below:

$$F_{BothTide} = \left(F_{high} \times t_{inundated}\right) + \left(F_{low} \times (24 - t_{inundated})\right) \quad (2)$$

$$F_{LowTide} = F_{low} \times 24 \quad (3)$$

where F_{low} and F_{high} are the average fluxes during low and high tides, respectively, $t_{inundated}$ is the average inundation time per day, acquired by multiplying the hours per day when the water level was higher than 0 cm by 2, since the tides are semidiurnal tides.

2.3 Statistical analysis

All the statistical analyses were performed in R 4.2.2 software. All the data were assessed for a normal distribution using the Shapiro–Wilk test. The nonparametric Wilcoxon rank sumKruskal–Wallis test one-way ANOVA on ranks was used to evaluate the differences in the CO_2 and CH_4 fluxes between sitesthe species. To determine which study sites differed, Dunn's multiple comparison test was applied as a post-hoc analysis when significantthe differences were significantdetected ($p < 0.05$). The relationships between the CO_2 and CH_4 fluxes during rising and falling tides were analyzed via a simple linear regression model. The results were considered statistically significant when the p value was lower than< 0.05. Data are primarilymainly presentedprimarily presented as the mean ± standard deviation (SD).

3 Results

During the study period, the mangrove tree stems served as both net CO_2 and CH_4 sources, but there was distinct species variation between sites (Fig. 2). In the *K. obovata* mangroves forest, tThe average CO_2 fluxes from the mangrove tree stems during the tidal cycle were 1.2113 ± 0.107 mmol m^{-2} h^{-1} at the K-WZW site and 1.0614.22 ± 0.208.21 mmol m^{-2} h^{-1} for *K. obovata* and *A. marina* at the K-XF site, respectively (Fig. 2a). The stem CO_2 fluxes were significantly higher at the A-FY and

已設定格式: 下標
已設定格式: 上標
已設定格式: 下標
已設定格式: 上標
已設定格式: 上標
已設定格式: 上標
已設定格式: 上標
已設定格式: 上標
已設定格式: 下標
已設定格式: 下標
格式化: 靠右
已設定格式: 字型: 非斜體
已設定格式: 下標
已設定格式: 下標
已設定格式: 下標
已設定格式: 英文 (英國)
已設定格式: 字型: 斜體
已設定格式: 字型: 斜體
已設定格式: 字型: 斜體
已設定格式: 下標

A-BM sites, averaging 10.62 ± 2.35 mmol m^{-2} h^{-1} and 16.00 ± 9.41 mmol m^{-2} h^{-1}, respectively (Fig. 2a). Across all sites, only the tree stem at the A-FY site functioned as a net CH_4 sink (-0.17 ± 0.52 μmol m^{-2} h^{-1}). However, the stem CH_4 fluxes ~~at~~of the K-WZW and K-XF sites showed no significant difference from the A-FY site, averaging 0.05 ± 0.06 μmol m^{-2} h^{-1} and 0.04 ± 0.04 μmol m^{-2} h^{-1}, respectively ~~The average CH_4 fluxes from the mangrove tree stems were 0.04 ± 0.05 μmol m^{-2} h^{-1} and 0.27 ± 1.05 μmol m^{-2} h^{-1} for *K. obovata* and *A. marina*, respectively~~ (Fig. 2b). The stem CH_4 fluxes were significantly higher at the A-BM site (0.48 ± 1.17 μmol m^{-2} h^{-1}; Fig. 2b). Compared to those of the tree stems, the soils of the *K. obovata* and *A. marina* mangrove forests ~~re~~exhibited remarkedly higher CH_4 fluxes, averaging 7.59 ± 8.74 μmol m^{-2} h^{-1} and 42.23 ± 62.95 μmol m^{-2} h^{-1}, respectively. The average CO_2 flux from the soil was 1.73 ± 2.31 mmol m^{-2} h^{-1} in the *K. obovata* mangroves ~~forest~~ and 3.42 ± 3.36 mmol m^{-2} h^{-1} in the *A. marina* mangroves ~~forest~~ but did not differ significantly from that from the tree stems.

已設定格式: 下標

已設定格式: 下標

已設定格式: 下標

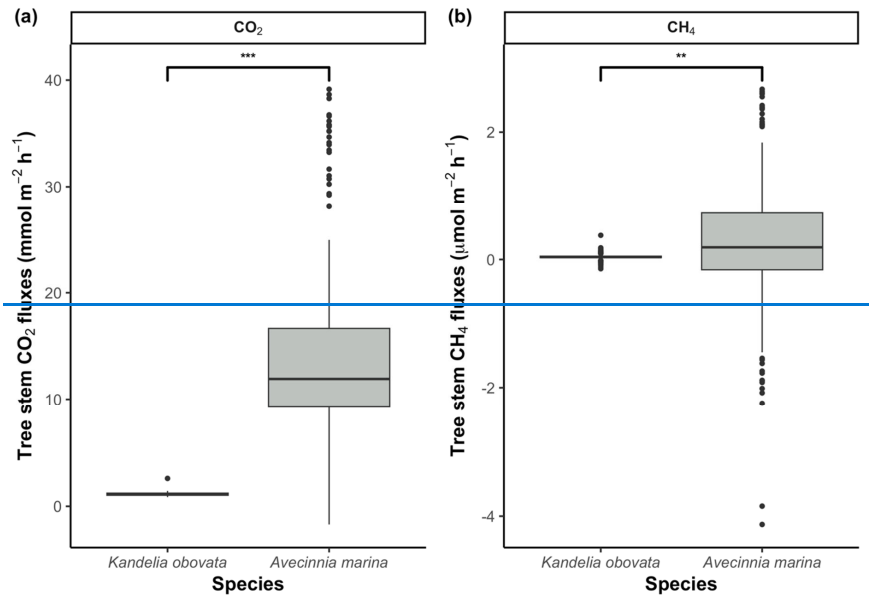
(a)
CO2
***
Tree stem CO2 fluxes (mmol m−2 h−1)
40
30
20
10
0
Kandelia obovata
Avecinnia marina
Species
(b)
CH4
**
Tree stem CH4 fluxes (μmol m−2 h−1)
2
0
-2
-4
Kandelia obovata
Avecinnia marina
Species

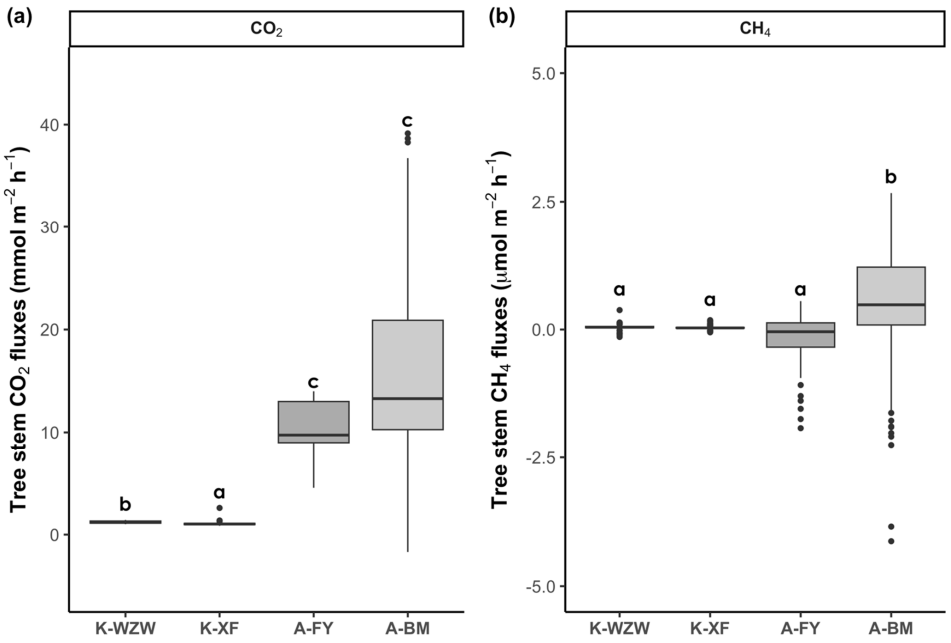

Figure 2. Difference in the tree stem (a) CO_2 and (b) CH_4 fluxes among~~between each~~ sites ~~*Kandelia obovata* and *Avicennia marina*~~**. Each data point represents a flux measurement during the tidal cycle (**K-WZW~~*K. obovata*~~**: ~~170~~ 88 replicates; K-XF: 82 replicates; A-FY~~*A. marina*~~**: ~~75~~227 replicates; A-BM: 152 replicates**). Different letters above the boxplot indicate significant differences among sites. ~~The label (*) indicates a statistically significant difference between the species,~~ as determined by the ~~nonparametric~~ Kruskal-Wallis test and Dunn's test ~~Wilcoxon rank sum test~~ (~~*~~: p<0.0~~015~~05; **: p<0.01; ***: p<0.001).**

The mean inundation time and ~~largest~~ highest tidal height at each sampling site are provided in Table 1. During the tidal cycle, the CO_2 fluxes from the mangrove tree stems exhibited different trends ~~depending on the species~~across all sampling sites (Fig. 3). The emissions remained relatively constant during the tidal cycle, ranging from 1.01 to 1.43 mmol m^{-2} h^{-1} and from 0.85 to 2.59 mmol m^{-2} h^{-1} at the K-WZW and K-XF sites, respectively (Fig. 3a). However, a sharp emission peak (2.59 mmol m^{-2} h^{-1}) was observed at the K-XF site on Day 2 when the tide was falling, which was three-fold higher than the lowest flux (0.85 mmol m^{-2} h^{-1}) measured on the same day (Fig. 3a). Similar to that at~~of~~ the K-WZW and K-XF sites~~*K. obovata*~~, the CO_2 flux at the A-FY and A-BM sites~~of *A. marina*~~ generally showed an increasing trend throughout the tidal cycle, ranging from 4.54 to 14.00 mmol m^{-2} h^{-1} and from -1.68 to~~:~~ 39.15 mmol m^{-2} h^{-1} ~~at the A-FY and A-BM sites~~, respectively (Fig. 3a). However,

this trend was observed at the A-FY site only on Day 1, when there was a distinct temporal trend in the increase in the CO_2 flux relative to that at the A-BM site. Specifically, the former started to increase before the flood current entered and stabilized after high tide, reaching a peak flux (10.36 mmol m^{-2} h^{-1}) at the end of the measurement. Conversely, the latter showed no significant change during the rising tide, followed by a steep rise toward high tide and a slight decrease during the falling tide; however, the CO_2 flux still remained higher than that during the preflood tide, ranging from -1.68 to 33.24 mmol m^{-2} h^{-1} during the rising tide and from 8.74 to 39.15 mmol m^{-2} h^{-1} during the falling tide (Fig. 3a).

Table 1. Comparison of the upscaling methods with and without considering tidal influences on the CO_2 and CH_4 fluxes of mangroves.

		K-WZW	K-XF	A-FY	A-BM
Dominant mangrove species		*Kandelia obovata*	*Kandelia obovata*	*Avecinnia marina*	*Avecinnia marina*
Sampling date		2022-07-14/2022-07-16	2022-06-15/2022-06-17	2022-06-01/2022-06-02, 2022-06-18	2022-07-27/2022-07-29
Sampling time		08:00/15:00	08:30/15:00	10:00/16:30	04:30/15:00
Mean inundation time (h)		6.69	6.69	5.19	15.33
Mean highest tidal height (cm)		58.160.0	73.570.5	47.362.0	77.583.0
Flux measurement number (n)		88	82	75	152
Stem CO_2 flux (mmol m^{-2} d^{-1})	$F_{BothTide}$ Tide	28.9339.00	25.0243	25248.880.39	3371.9523.52
	$F_{LowTide}$ None	28.9429.35	24.8225.13	245.95254.80	339.99570.42
	Difference (%)	0.031.20	0.811.19	1.191.75	9.4055.24
Stem CH_4 flux (μmol m^{-2} d^{-1})	$F_{BothTide}$ Tide	1.180	0.819	-5.044.31	8.170.40
	$F_{LowTide}$ None	1.2213	0.7691	-5.494.11	-0.7424.47
	Difference (%)	2.693.68	2.226.21	8.354.75	193.571200.25
Mean soil CO_2 flux (mmol m^{-2} d^{-1})		27.26	57.13	134.19	57.09
Mean soil CH_4 flux (μmol m^{-2} d^{-1})		149.77	217.42	2404.28	345.37
Meangrove forest area (ha) [a]		150.86	98.3712	6835.7	5.4875.3
Mean tree height (m) [a]		4.0	5.1	1.8	3.2
Mean tree density (tree m^{-2}) [a]		1.3	2.4	1.0	0.6
Mean diameter at breast height (cm) [a]		7.0	5.6	10.5	6.2

已設定格式: 字型: 斜體

格式化表格

已設定格式: 上標

Stem lenticel density (lenticels cm^{-2})	0.08	0.05	1.83	2.96

$F_{BothTide}$~~Tide~~: The average fluxes during low and high tides were added after multiplication with the corresponding time length. $F_{LowTide}$~~None~~: The average fluxes during ~~a tidal cycle~~ low tides were multiplied by 24 hours. The sampling date and time are in ISO 8601 format.

[a] The data was derived from Lin et al. (2021).

The CO_2 flux pattern observed during the tidal cycle differed between the tree stems and soils. Generally, the soil CO_2 flux peaked before and after high tide at all sites, either during the rising or falling tide, with the flood current just entering or leaving the sampling site (Fig. 3b).

格式化: 間距 套用後: 0 點

已設定格式: 上標

已設定格式: 英文 (美國)

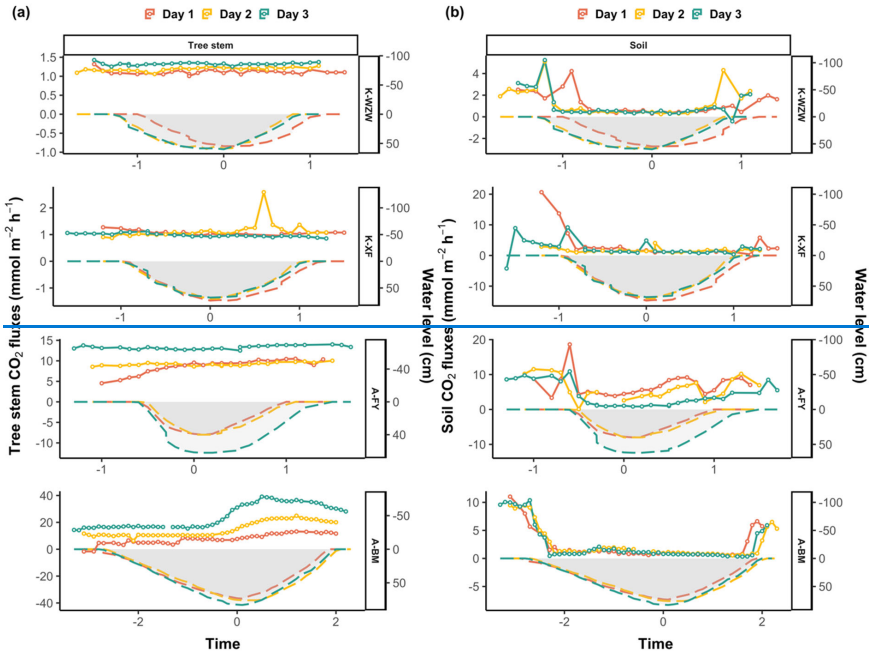
(a)
Day 1
Day 2
Day 3
Tree stem
K-WZW
K-XF
A-FY
A-BM
Tree stem CO_2 fluxes (mmol m^{-2} h^{-1})
Water level (cm)
Time
(b)
Soil
Soil CO_2 fluxes (mmol m^{-2} h^{-1})
Water level (cm)
Time

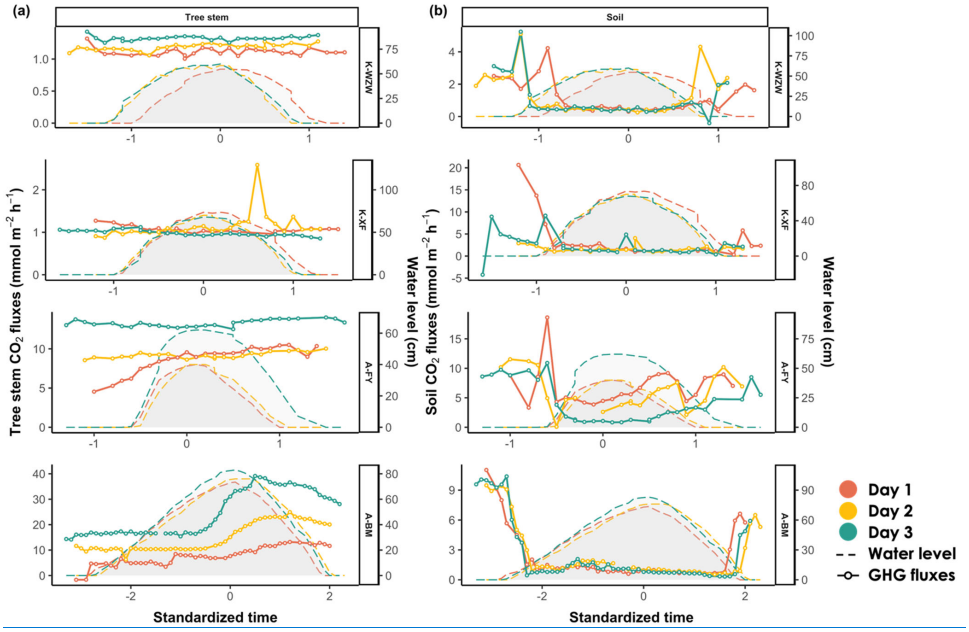

Figure 3. Variations in (a) the tree stem CO_2 fluxes and (b) soil CO_2 fluxes during the tidal cycle. The time was standardized based on the time of the highest water level during the high-tide period (set as 0), then adjusted by decrementing the time by 0.1 for every 10-minute interval prior to the peak and incrementing by 0.1 for every 10-minute interval after the peak. The average values of the flux and water level were calculated when falling within each standardized time interval. The shaded area denotes the water level at the sampled tree. On Days 1, 2, and 3, the plant data were arranged chronologically according to the sampling date.

Similar to those in the CO_2 flux, the CH_4 fluxes of *K. obovata* and *A. marina* exhibited distinct temporal trends during the tidal cycle (Fig. 4). In the *K. obovata* mangroves ~~forest~~, there was significant variation in the stem CH_4 flux during the tidal cycle, ranging from -0.14 to 0.38 μmol m^{-2} h^{-1} ~~(0.05 ± 0.06 μmol m^{-2} h^{-1})~~ and from -0.05 to 0.18 μmol m^{-2} h^{-1} ~~(0.04 ± 0.04 μmol m^{-2} h^{-1})~~ at the K-WZW and K-XF sites, respectively, while consistent patterns were lacking between each sampling campaign (Fig. 4a). The stem CH_4 flux of *A. marina* increased throughout the tidal cycle, ranging from -1.92 to 0.55 μmol m^{-2} h^{-1} ~~(-0.17 ± 0.52 μmol m^{-2} h^{-1})~~ and from -4.13 to 2.67 μmol m^{-2} h^{-1} ~~(0.48 ± 1.17 μmol m^{-2} h^{-1})~~ at the A-FY and A-BM sites, respectively. Specifically, the tree stems of *A. marina* functioned as CH_4 sinks before tidal inundation (A-FY: -0.538 ± 0.7341.14 μmol m^{-2} h^{-1}; A~~:~~-BM: -0.64 ± 1.51 μmol m^{-2} h^{-1}), but the CH_4 flux gradually increased thereafter, eventually becoming a CH_4 source during low tide (A-FY: 0.180.60 ± 0.274 μmol m^{-2} h^{-1}; A-BM: 1.54 ± 0.56 μmol m^{-2} h^{-1}). However, this pattern was not observed across all sampling campaigns (Fig. 4a).

For both mangrove species, the soil CH_4 flux during high tide (21.65 ± 45.29 μmol m^{-2} h^{-1}) was lower than that during low tide (47.70 ± 63.27 μmol m^{-2} h^{-1}) (Fig. 4b). Furthermore, there was a peak in the soil CH_4 flux during both tidal increase and decrease on all three sampling days, similar to the soil CO_2 flux (Fig. 3b; Fig. 4b).

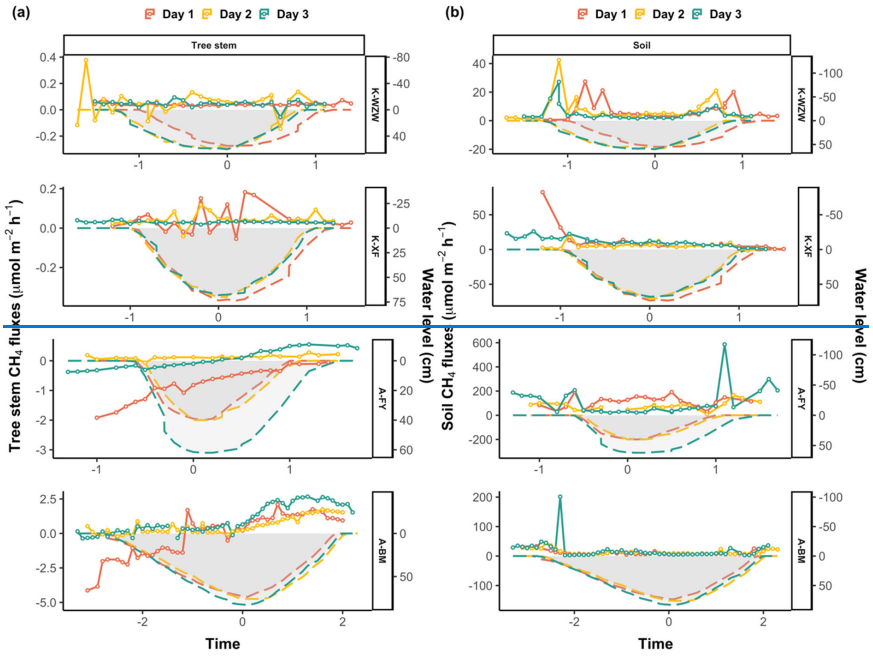
(a)
Day 1
Day 2
Day 3
Tree stem
K-WZW
K-XF
A-FY
A-BM
Tree stem CH4 fluxes (μmol m-2 h-1)
Water level (cm)
Time
(b)
Soil
Soil CH4 fluxes (μmol m-2 h-1)
Water level (cm)
Time

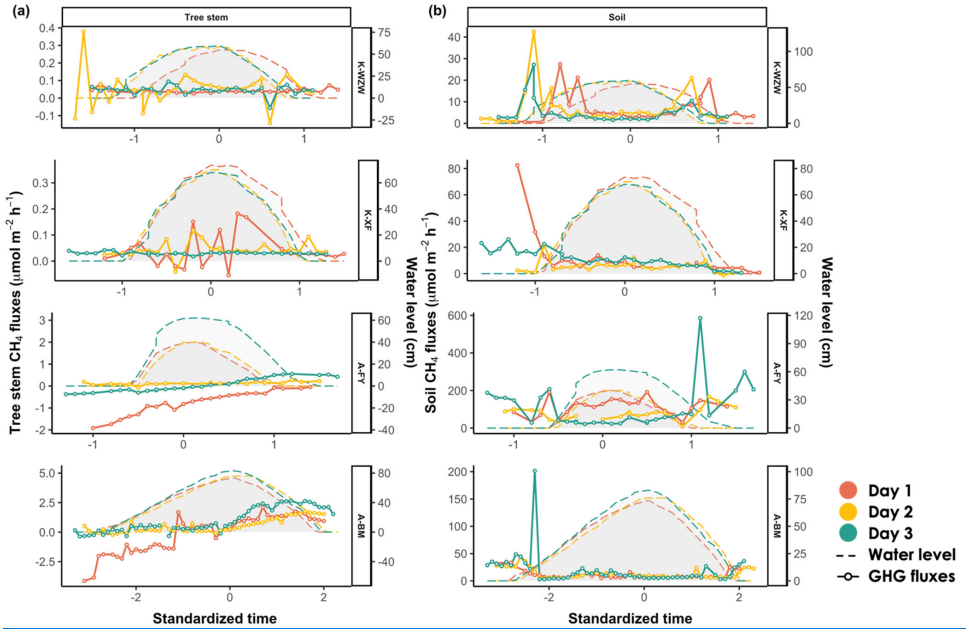

Figure 4. Variations in (a) the tree stem CH_4 fluxes and (b) soil CH_4 fluxes during the tidal cycle. The time was standardized based on the time of the highest water level during the high-tide period (set as 0), then adjusted by decrementing the time by 0.1 for every 10-minute interval prior to the peak and incrementing by 0.1 for every 10-minute interval after the peak. The average values of the flux and water level were calculated when falling within each standardized time interval. The shaded area denotes the water level at the sampled tree. On Days 1, 2, and 3, the plant data were chronologically arranged according to the sampling date.

During the tidal cycle, the CO_2 flux from the mangrove tree stems was positively correlated with the CH_4 flux during both the rising and falling tides. However, a significant relationship was detected only for *A. marina* (Fig. 5a; $p<0.001$). The CO_2 and CH_4 fluxes from both the stems and soils were simultaneously measured, and a negative correlation between the stem and soil fluxes was observed across the two mangrove species. However, a significant relationship was detected only for *A. marina* during the falling tide (Fig. 5b, 5c; $p<0.001$).

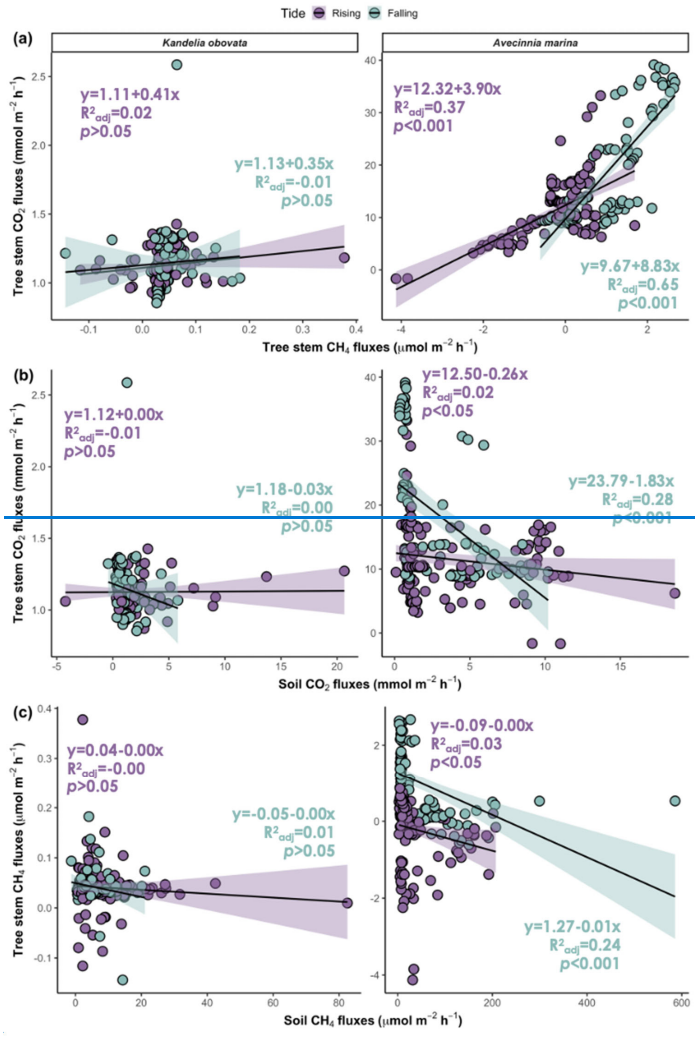
Tide Rising Falling
(a)
Kandelia obovata
Avecinnia marina
y=1.11+0.41x
R²adj=0.02
p>0.05
y=1.13+0.35x
R²adj=-0.01
p>0.05
y=12.32+3.90x
R²adj=0.37
p<0.001
y=9.67+8.83x
R²adj=0.65
p<0.001
Tree stem CO2 fluxes (mmol m-2 h-1)
Tree stem CH4 fluxes (μmol m-2 h-1)
(b)
y=1.12+0.00x
R²adj=-0.01
p>0.05
y=1.18-0.03x
R²adj=0.00
p>0.05
y=12.50-0.26x
R²adj=0.02
p<0.05
y=23.79-1.83x
R²adj=0.28
p<0.001
Tree stem CO2 fluxes (mmol m-2 h-1)
Soil CO2 fluxes (mmol m-2 h-1)
(c)
y=0.04-0.00x
R²adj=-0.00
p>0.05
y=-0.05-0.00x
R²adj=0.01
p>0.05
y=-0.09-0.00x
R²adj=0.03
p<0.05
y=1.27-0.01x
R²adj=0.24
p<0.001
Tree stem CH4 fluxes (μmol m-2 h-1)
Soil CH4 fluxes (μmol m-2 h-1)

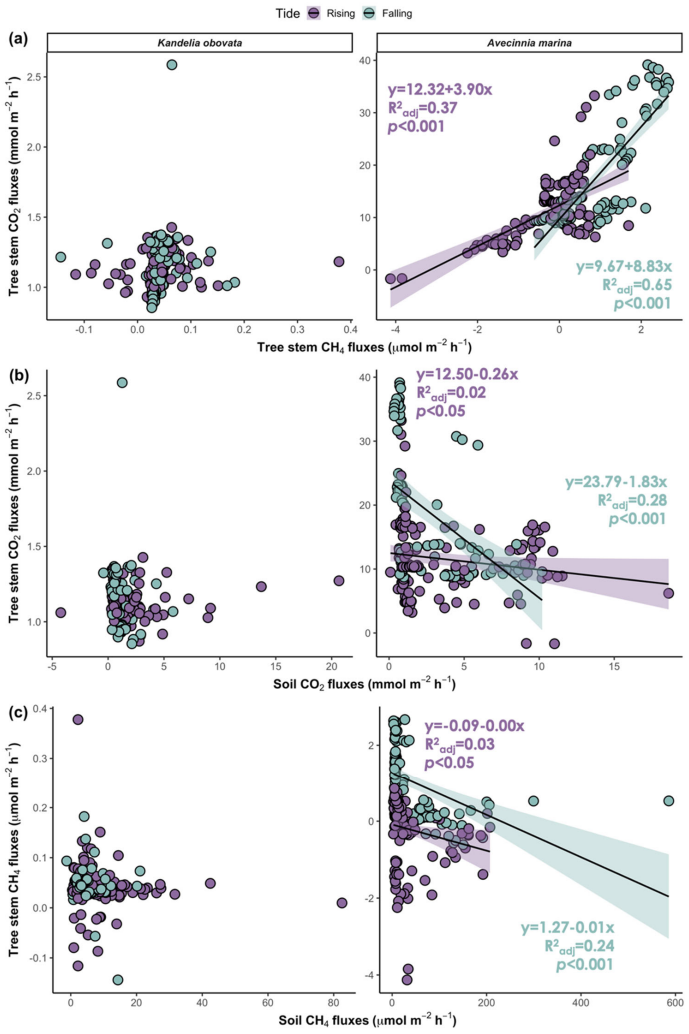

Figure 5. Relationships between (a) the tree stem CO_2 and CH_4 fluxes, (b) tree stem CO_2 fluxes and soil CO_2 fluxes, and (c) tree stem CH_4 fluxes and soil CH_4 fluxes. The shaded areas denote the 95% confidence intervals of the regression lines.

Since the tides at the sample sites were mainly semidiurnal tides, the average inundation time per day was calculated from the average time of high tide (when the water level was higher than 0 cm) during each sampling event multiplied by 2. The A-BM site exhibited the longest inundation time of 15.33 hours, while the inundation time during the sampling campaign was 6.69 hours at the K-WZW and K-XF sites and 5.19 hours at the A-FY site. The ~~largest~~ average highest tidal height (determined by the distance between the soil and water surface during high tide) was ~~60~~ 58.1 cm at the K-WZW site, ~~74~~ 70.5 cm at the K-XF site, ~~62~~ 47.3 cm at the A-FY site, and ~~83~~ 77.5 cm at the A-BM site. Different upscaling methods were applied to determine the tidal influence on the diurnal variation in the fluxes, where "$F_{BothTide}$~~tide~~" denotes the sum of the average fluxes during low and high tides after multiplication with the corresponding time length, and "$F_{LowTide}$~~none~~" denotes the average flux during ~~the tidal cycle~~low tides multiplied by 24 hours. The GHG fluxes exhibited notable differences when tidal influences were considered (Table 1). Based on our findings, sampling only during low tide could ~~cause~~ under~~over~~estimat~~ion of~~e the stem CO_2 and CH_4 fluxes on a diurnal scale, except at the K-WZW site., where the stem CO_2 and CH_4 fluxes were 0.03% and 3.68% lower when considering tidal influences (Table 1). At the K-XF, A-FY and A-BM sites, t~~T~~he differences in the stem CO_2 ~~and CH_4~~ fluxes ~~of *K. obovata*~~ between the upscaling methods were smaller than those in the stem CH_4 fluxes ~~of *A. marina*~~, ranging from 0.81%~~1.19~~ to 9.40~~2.69~~% (Table 1). The stem CH_4 fluxes at the K-XF site were approximately 6% higher when considering tidal influences, as opposed to ignoring tidal influences ~~However, the stem CO_2 flux of *A. marina* varied by approximately 60% when considering tidal influences, as opposed to ignoring tidal influences~~ (Table 1). If the tidal influences were not accounted for, the mangrove tree stems ~~Tidal influences also imposed a significant effect on the stem CH_4 flux~~ at the A-FY and A-BM sites both acted as net CH_4 sink~~of *A. marina*~~, while the CH_4 sink capacity was ~~resulting in the highest variation of~~ 8% and ~~194~~1200% lower after ~~relative to not~~ accounting for tidal influences, turning the mangrove tree stem at the A-BM site into a net CH_4 source (Table 1).

已設定格式: 下標
已設定格式: 下標
已設定格式: 下標
已設定格式: 下標
已設定格式: 下標
已設定格式: 下標
已設定格式: 下標

4 Discussion

This study revealed distinct ~~species~~ spatial and temporal variations in the CO_2 and CH_4 fluxes originating from tree stems and soils. Specifically, ~~the sample~~ sites dominated by *A. marina* exhibited ~~significantly~~ up to 15 times higher CO_2 ~~and CH_4~~ fluxes than sites dominated by *K. obovata*. The tree stems of *A. marina* at the A-FY site acted as a net CH_4 sink, while the A-BM site emitted CH_4 at approximately three times higher ~~flux~~ rate. In contrast, the tree stems of *K. obovata* at the K-WZW and K-XF sites were a weak CH_4 source compared to the tree stem at the A-BM site. ~~, suggesting that *A. marina* may play a more prominent role in GHG dynamics than *K. obovata*.~~ The temporal dynamics during the tidal cycle also differed between the two mangrove species. Regarding *K. obovata*, the stem CO_2 and CH_4 fluxes at the K-WZW and K-XF sites lacked a consistent pattern between each sampling campaign. In contrast, *A. marina* exhibited an increasing trend in the CO_2 flux throughout the tidal cycle, whereas the CH_4 flux exhibited high temporal variability, functioning as a sink before tidal inundation and becoming a source during low tide at both A-FY and A-BM sites. Therefore, our results ~~indicated~~ suggest~~ed~~ that the different

已設定格式: 字型: (英文)Times New Roman
已設定格式: 字型: 斜體
已設定格式: 下標
已設定格式: 下標
已設定格式: 字型: 斜體
已設定格式: 下標

mangrove species, in this case, *K. obovata* and *A. marina*, may provide varying capacities for CO_2 and CH_4 exchange with the atmosphere through the tree stems during tidal cycles. Further investigation with a larger sample size ~~of each species s~~ neededeessary to examinevalidate theis hypothesis of mangrove species variation in GHG flux.

In terms of biological factors, *A. marina* contains pneumatophores, while *K. obovata* does not. Pneumatophores may facilitate the transport of oxygen to the rhizosphere and increase the oxidation–reduction potential, thereby inhibiting the methanogenesis process (Dušek et al., 2021). However, they can also serve as pathways for deep soil layer CH_4 emissions, facilitating CH_4 transport (He et al., 2019; Lin et al., 2021). In this study, pneumatophores were not intentionally avoided during the measurement. Therefore, the presence of pneumatophores may contribute to the increased soil CH_4 flux in the *A. marina* mangrove forest.

The GHG emissions of the stem, whether originating from the soil or the stem itself, require radial diffusion through the bark or lenticel to reach the atmosphere (Barba et al., 2019a). Radial diffusion is primarily influenced by biological factors such as wood density, wood moisture content, and lenticel density (Covey and Megonigal, 2019). A higher lenticel density, in particular, creates more pathways for GHG emissions, resulting in increased emissions (Zhang et al., 2022). Based on visual observation in situ, we found that the tree stems at the A-FY and A-BM sites ~~*A. marina*~~ exhibited a significantly higher lenticel density than those at the K-WZW and K-XF sites ~~*K. obovata*~~ (Table 1). Therefore, it is speculated that the higher lenticel density of *A. marina* facilitates the emission of GHGs from the stem, resulting in a higher stem GHG flux at the A-FY and A-BM sites.~~.~~

Previous studies on GHG emissions originating from mangrove tree stems were mostly conducted during low tide and under daylight conditions. Gao et al. (2021) showed that the stems of *Kandelia obovata* can both absorb and release CH_4, with average fluxes of -5.69 and 1.84 μmol m^{-2} h^{-1}, respectively. Zhang et al. (2022) reported higher CH_4 emissions from *K. obovata* stems (7.04 μmol m^{-2} h^{-1}), which dominated the ecosystem CH_4 flux of mangroves without pneumatophores. This contradicts the findings of this study, where the CH_4 emissions of *K. obovata* stems contributed less than the soil emissions. Liao et al. (2024) measured lower stem CH_4 fluxes from *K. obovata* during the winter ~~season~~ (0.54 μmol m^{-2} h^{-1}), which were 10 ~~still~~ times higher than the average fluxes observed in this study. In the case of *A. marina*, the average stem CH_4 fluxes were 1.56 μmol m^{-2} h^{-1} (Jeffrey et al., 2019) and 2.79 μmol m^{-2} h^{-1} (Zhang et al., 2022) at the mangrove sites located in Australia and China, respectively. The tree stems of *A. marina* also exhibited CH_4 consumption capacity, with fluxes ranging from -33.96 to 48.83 μmol m^{-2} h^{-1}, as reported in Gao et al. (2021). Regarding other mangrove species, *Kandelia candel* exhibited a stem CH_4 flux of -1.81 μmol m^{-2} h^{-1}, while *Sonneratia apetala*, *Laguncularia racemosa*, and *Bruguiera gymnorhiza-Bruguiera sexangula*, which have the same specialized root structure as that of *A. marina*, provided stem CH_4 fluxes of 2.62, 0.87, and -0.49 μmol m^{-2} h^{-1}, respectively (He et al., 2019). Epron et al. (2023) measured the CH_4 flux of the stems of *Bruguiera gymnorrhiza* throughout a 24-hour cycle, which ranged from -0.360.02 to 263.16.63 μmol m^{-2} h^{-1}. In this study, the CH_4 fluxes of the stems of *A. marina* and *K. obovata* ranged from -0.14 to 0.38 μmol m^{-2} h^{-1} (K-WZW: 0.05 ± 0.06 μmol m^{-2} h^{-1}; K-XF:

已設定格式: 下標
已設定格式: 字型: 斜體
已設定格式: 上標
已設定格式: 非上標/ 下標
已設定格式: 字型: 斜體
已設定格式: 下標

0.04 ± 0.04 μmol m^{-2} h^{-1}) and from -4.13 to 2.67 μmol m^{-2} h^{-1} (A-FY: -0.17 ± 0.52 μmol m^{-2} h^{-1}; A-BM: 0.48 ± 1.17 μmol m^{-2} h^{-1}), respectively, which were at the low end of the reported range of ~~reported~~ stem CH_4 fluxes in previous studies (Table 2). Although CH_4 fluxes from mangrove tree stems generally decreased with increasing height (Epron et al., 2023; Gao et al., 2021; Jeffrey et al., 2019; Liao et al., 2024), average stem CH_4 fluxes of *A. marina* and *K. obovata* within similar heights to this study (> 1 m) were still higher. This may be due to site-specific variations in environmental conditions, tree physiology, and microbial activity, all of which can influence the production and consumption of methane by mangrove trees (Barba et al., 2019a; Covey and Megonigal, 2019). Further research is ~~neededecessary~~ to delve into the underlying mechanisms which were not fully elucidated in this study due to ~~the~~ limited data availability~~le~~. ~~Herein, *K. obovata* and *A. marina* served as net CH_4 sources rather than sinks, while both species exhibited lower CH_4 emissions than those obtained in previous studies focused on the same species. *A. marina* also exhibited higher variability and a higher capacity for CH_4 sequestration.~~

Table 2. Comparision of tree stem methane (CH_4) flux in mangrove ~~forest~~ ecosystems reported in this study with previous literature ~~and this study~~. The values were presented as the range (minimum value–maximum value) and ~~(~~mean ± standard deviation~~)~~.

Site	Period	Species	Height (m)	Stem CH_4 fluxes (μmol m^{-2} h^{-1})	Measurement technique	Reference
Australia	Winter (Aug 2018)	*A. marina*	0.12	0.01–21.00 (4.03 ± 1.15)	CRDS	Jeffrey et al. (2019)
			0.4	0.03–6.84 (1.21 ± 0.30)		
			0.8	0.31–4.77 (1.25 ± 0.19)		
			1.51	0.51–2.62 (1.14 ± 0.10)		
China	All (Feb 2012–Nov 2013)	*L. racemosa* *S. apetala* *K. candel* *B. gymnorhiza-sexangula*		0.87 ± 0.81 2.61 ± 1.25 -1.81 ± 1.00 -0.49 ± 0.75	GC	He et al. (2019)
	Summer (Jul 2019–Aug 2019)	*K. obovata* (Site 1)	0.4	-78.78–11.35 (-7.12)	CRDS	Gao et al. (2021)
			1.4	-52.67–8.89 (-4.39)		
		K. obovata (Site 2)	0.4	-32.36–26.90 (2.97)		
			1.4	-9.95–51.38 (1.63)		
		A. marina	0.4	-33.96–22.50		
			1.4	-23.34–48.83		
		A. corniculatum	0.4	-131.19–225.16		
			1.4	-41.42–42.43		
	Winter (Jan 2018), Summer (Jul 2018)	*K. obovata* *A. corniculatum* *A. marina*	0–1.25	(7.04 ± 3.96) (5.42 ± 3.04) (2.79 ± 2.13)	GC	Zhang et al. (2022)
	Winter (Dec 2021–Mar 2021)	*K. obovata*	0.7	(0.68 ± 0.17)		Liao et al. (2024)
			1.2	(0.57 ± 0.19)		
			1.7	(0.37 ± 0.13)		

已設定格式: 非上標/ 下標
已設定格式: 下標
已設定格式: 下標
已設定格式: 下標
格式化: 標號
已設定格式: 下標
已設定格式: 字型: Times New Roman
已設定格式: 字型: Times New Roman
已設定格式: 字型: (英文)Times New Roman
已設定格式: 英文 (美國)
格式化: 行距: 單行間距
格式化表格
格式化: 行距: 單行間距
格式化: 行距: 單行間距
格式化: 行距: 單行間距
格式化: 行距: 單行間距
格式化: 行距: 單行間距
格式化: 行距: 單行間距
格式化: 行距: 單行間距
格式化: 行距: 單行間距
格式化: 行距: 單行間距
格式化: 行距: 單行間距
格式化: 行距: 單行間距
格式化: 行距: 單行間距
格式化: 行距: 單行間距
格式化: 行距: 單行間距

		S. apetala	0.7	(1.25 ± 0.21)		
			1.2	(0.84 ± 0.14)		
			1.7	(0.42 ± 0.12)		
Japan	Summer (July 2022)	*B. gymnorrhiza*	0.3	1.80–825.12 (143.64)		Epron et al. (2023)
			0.6–1.5	-0.36–263.16 (30.6)		
Taiwan	Summer (Jun 2022–Jul 2022)	*K. obovata* (K-WZW)	1.1	-0.14–0.38 (0.05 ± 0.06)	CEAS	This study
		K. obovata (K-XF)		-0.05–0.18 (0.04 ± 0.04)		
		A. marina (A-FY)		-1.92–0.55 (-0.17 ± 0.52)		
		A. marina (A-BM)		-4.13–2.67 (0.48 ± 1.17)		

GC: Gas chromatography; CRDS: Cavity ring-down spectroscopy; CEAS: Cavity-enhanced absorption spectroscopy.

The tree stem CO_2 and CH_4 fluxes exhibited similar temporal patterns during the tidal cycle. A significant positive relationship was also found between these fluxes, indicating that CO_2 and CH_4 emitted by mangrove tree stems may originate from the same source or be influenced by the same mechanism during the tidal cycle (Liao et al., 2024). According to previous studies, CO_2 emissions primarily occur through root respiration and stem respiration, as well as internal plant metabolism and transport from soils (Teskey et al., 2008). In contrast, CH_4 may be emitted or absorbed by methanogens and methanotrophs present in tree bark or heartwood (Feng et al., 2022; Jeffrey et al., 2021). CH_4 emitted by tree stems may also originate from the soil, where the CH_4 produced in the soil enters the root system, enters the tree aerenchyma tissues or xylem, and is subsequently directly released into the atmosphere through the lenticel or tree stems (Barba et al., 2019a; Covey and Megonigal, 2019). Therefore, the ~~emission~~ fixation ~~and absorption~~ of CO_2, oxidation of ~~and~~ CH_4, and emission of both GHGs by the tree stem may originate from the tree stem itself or from the soil. In this study, the transformation of tree stems from CH_4 sinks to CH_4 sources was observed in the *A. marina* mangrove forest. This observation indicates that CH_4 emitted by tree stems may be affected by different sources during different periods of the tidal cycle.

The transport mechanism of GHGs in the stem is similar to that of herbaceous plants, occurring mainly by diffusion or evaporation, either jointly or individually. The diffusion direction mainly depends on the CH_4 concentration gradient. For example, if the gas concentration in the rhizosphere is high, GHGs can enter the plant root system either in gaseous or liquid form, thus entering the aerenchyma or xylem tissue (Vroom et al., 2022). Aerenchyma is a specialized tissue found in many mangrove tree species (Evans, 2004). It comprises air-filled spaces that create gas transport pathways within the plant. Aerenchyma facilitates gas movement, including CO_2 and CH_4, within stems. Within the aerenchyma, CO_2 and CH_4 can diffuse or passively flow along concentration gradients. This transport pathway allows gases to move vertically within the plant, from the roots through the stem and ultimately into the atmosphere. Aerenchyma tissue is particularly important for CH_4 transport because CH_4 is produced in oxygen-limited soils or in the rhizosphere by methanogens. The aerenchyma provides a direct

已設定格式: 字型: 斜體
格式化: 行距: 單行間距
格式化: 行距: 單行間距
格式化: 行距: 單行間距
格式化: 行距: 單行間距
格式化: 行距: 單行間距
格式化: 行距: 單行間距
格式化: 行距: 單行間距
格式化: 行距: 單行間距
格式化: 行距: 單行間距
格式化: 標號

pathway for CH_4 to move upward through the stems to be emitted into the atmosphere (Yáñez-Espinosa and Angeles, 2022). CO_2 and CH_4 can also dissolve during dilution and be transported within the xylem via sap flux (Takahashi et al., 2022).

This study revealed the transition of mangrove tree stems from CH_4 sinks to CH_4 sources within the tidal cycle, which has not been observed in other studies, even with a high measurement frequency of upland tree stems at one-hour intervals (Barba et al., 2019b). We speculate that the tree stem of *A. marina* may absorb CH_4 through the presence of methanotrophs during low tide (Jeffrey et al., 2021). During inundation, the diffusion of CH_4 produced in the deep soil layer may be restricted by the water pressure (Tong et al., 2013) since the pore spaces are filled with water. Tong et al. (2010) also reported a significantly lower CH_4 flux during inundation than during low tide. Therefore, we hypothesize that CH_4 produced in the soil during inundation periods may be primarily emitted into the atmosphere through tree stems (Vroom et al., 2022; Yáñez-Espinosa and Angeles, 2022) rather than being emitted across the water–atmosphere interface via diffusion or ebullition (Li et al., 2021), resulting in the observed gradual increase in the CH_4 flux throughout the tidal cycle. This hypothesis was also supported by the negative relationship between the soil and stem CH_4 fluxes of *A. marina* during both rising and falling tides observed in this study. However, the CH_4 flux of the tree stems of *Bruguiera gymnorrhiza* peaked after the tide receded (Epron et al., 2023), which does not support this hypothesis. It is critical to note that the specific mechanisms driving the observed peaks may vary depending on factors such as mangrove species, environmental conditions, tidal dynamics, and site-specific characteristics. However, further research is necessary to fully comprehend the underlying mechanisms.

To our knowledge, this study is the first to simultaneously measure the CH_4 fluxes of both stems and soils throughout the tidal cycle, even during tidal inundation. When quantifying the GHG emissions of mangrove tree stems, the discrete and continuous methods are two common measurement approaches. Discrete measurements involve sampling at specific time points with a lower temporal resolution but are practical and cost effective. Continuous measurements provide real-time monitoring with a high temporal resolution, accurately capturing short-term fluctuations and peak emissions but requiring specialized equipment and technical expertise. When considering tidal influences through continuous measurements, the ~~GHGs methane~~CH_4 emitted by mangrove tree stems were significantly ~~lower~~higher, with differences of up to ~~60% and 1~~20094% for the stem ~~CO_2 and~~ CH_4 fluxes~~, respectively~~. Conversely~~In tidal salt marshes~~, the upscaled CH_4 flux ~~,~~ accounting for tides in tidal salt marshes~~,~~ was ~~also~~ lower (Huang et al., 2019). When quantifying the GHG emissions of mangrove tree stems, discrete measurements are commonly used due to sampling difficulty at night and high tide. Although discrete measurements can still provide reliable estimates of the average emission rate over a specific period, they are useful only for broader-scale quantification and carbon and CH_4 budgeting models. This study highlights the need for continuous measurements of the GHG fluxes in coastal ecosystems, which can provide a more detailed understanding of emission patterns, aid in overall emission quantification, help individuals identify key drivers and mechanisms, reduce the uncertainty in GHG emissions, and facilitate the assessment of the impacts of specific events or environmental variables (Capooci and Vargas, 2022). However, when comparing practical, feasible, and cost-effective discrete measurements, continuous measurements require specialized equipment, technical expertise and intensive labor. It should also be noted that considerable differences were mainly observed at the A-BM site, with the longest inundation and highest water table.

已設定格式: 字型: 斜體

已設定格式: 下標

This study provides insights into the potential tidal influence on ~~greenhouse gas (~~GHG~~)~~ fluxes from mangrove tree stems. However, several uncertainties require further investigation. First, the study was conducted during the summer ~~season~~ and daylight hours, which may have resulted in higher fluxes due to the effects of higher temperatures and the sap-flux dependent transport mechanism within the tree stems (Barba et al., 2019b; Köhn et al., 2021; Pangala et al., 2015; Pitz et al., 2018; Takahashi et al., 2022; Wang et al., 2016; Zhang et al., 2022). Second, the sampling campaign was conducted during spring tide, while CH_4 fluxes in tidal wetlands may differ between spring and neap tides (Huang et al., 2019; Tong et al., 2013). Third, sampling only at 110 cm height may have overlooked height-related GHG flux variations within mangrove tree stems, as observed in other~~related~~ studies (Epron et al., 2023; Jeffrey et al., 2019; Moldaschl et al., 2021; Pangala et al., 2013, 2014, 2015; Sjögersten et al., 2020). Finally, ~~Lastly,~~ with the limited data availability~~only one tree sampled per site~~, it is still uncertain whether there is a significant difference in GHG emissions from the tree stems between the two mangrove species.~~the representativeness of the findings may be insufficient~~.

已設定格式: 下標

已設定格式: 英文 (美國)

5 Conclusion

已設定格式: 英文 (美國)

This study revealed distinct ~~species~~ temporal variations in the CO_2 and CH_4 fluxes of the tree stems of *A. marina* and *K. obovata* throughout the tidal cycles. While the ~~The results demonstrated that *A. marina* exhibited significantly higher emissions of both CO_2 and CH_4 than *K. obovata*, indicating its potentially greater contribution to the assessment of the carbon budget. The temporal variation during the tidal cycle also differed, with~~GHG fluxes of *K. obovata* stems ~~lacking~~ displayed in~~a~~ consistent pattern, ~~and~~ the CH_4 ~~emissions~~ fluxes of *A. marina* stems suggesting a transition from a sink to a source, indicating the influence of different sources and mechanisms at different tidal phases. When considering tidal influences, the stem CH_4 flux could vary up to ~~19~~12004% for *A. marina*, turning the stem from a net CH_4 sink to a source.~~.~~ This study highlights the need to consider tidal influences when quantifying the GHG fluxes of mangrove tree stems and the potential limitations of discrete measurements relative to continuous measurements. However, further research is needed to fully understand the underlying mechanisms driving the observed flux variations and to improve our understanding and reduce the uncertainty in GHG dynamics in mangrove ecosystems.

已設定格式: 下標

Data availability. The original contributions presented in the study are included in the article. We encourage prospective data users to contact us before embarking on any analysis.

Author contributions. Zhao-Jun Yong: Methodology, Investigation, Visualization, Writing - Original Draft. Wei-Jen Lin: Methodology, Investigation, Visualization, Chiao-Wen Lin: Methodology, Investigation, Visualization. Hsing-Juh Lin: Conceptualization, Supervision, Writing – Review & Editing, Funding acquisition.

Competing interests. None of the authors declare any conflict of interest.

Acknowledgements. This study was financially supported by the Ministry of Science and Technology of Taiwan under grant no. 112-2621-M-005-004 to HJL, and the "Innovation and Development Center of Sustainable Agriculture" from The Featured Areas Research Center Program within the framework of the Higher Education Sprout Project by the Ministry of Education (MOE) of Taiwan.

References

Bahlmann, E., Weinberg, I., Lavrič, J. V., Eckhardt, T., Michaelis, W., Santos, R., and Seifert, R.: Tidal controls on trace gas dynamics in a seagrass meadow of the Ria Formosa lagoon (southern Portugal), Biogeosciences, 12, 1683–1696, https://doi.org/10.5194/bg-12-1683-2015, 2015.

Barba, J., Poyatos, R., and Vargas, R.: Automated measurements of greenhouse gases fluxes from tree stems and soils: Magnitudes, patterns and drivers, Sci. Rep., 9, 4005, https://doi.org/10.1038/s41598-019-39663-8, 2019a.

Barba, J., Bradford, M. A., Brewer, P. E., Bruhn, D., Covey, K., Haren, J., Megonigal, J. P., Mikkelsen, T. N., Pangala, S. R., Pihlatie, M., Poulter, B., Rivas-Ubach, A., Schadt, C. W., Terazawa, K., Warner, D. L., Zhang, Z., and Vargas, R.: Methane emissions from tree stems: A new frontier in the global carbon cycle, New Phytol., 222, 18–28, https://doi.org/10.1111/nph.15582, 2019b.

Billerbeck, M., Werner, U., Polerecky, L., Walpersdorf, E., deBeer, D., and Huettel, M.: Surficial and deep pore water circulation governs spatial and temporal scales of nutrient recycling in intertidal sand flat sediment, Mar. Ecol. Prog. Ser., 326, 61–76, https://doi.org/10.3354/meps326061, 2006.

Carmichael, M. J., Bernhardt, E. S., Bräuer, S. L., and Smith, W. K.: The role of vegetation in methane flux to the atmosphere: Should vegetation be included as a distinct category in the global methane budget?, Biogeochemistry, 119, 1–24, https://doi.org/10.1007/s10533-014-9974-1, 2014.

Covey, K. R. and Megonigal, J. P.: Methane production and emissions in trees and forests, New Phytol., 222, 35–51, https://doi.org/10.1111/nph.15624, 2019.

Capooci, M. and Vargas, R.: Trace gas fluxes from tidal salt marsh soils: Implications for carbon–sulfur biogeochemistry, Biogeosciences, 19, 4655–4670, https://doi.org/10.5194/bg-19-4655-2022, 2022.

Duarte de Paula Costa, M. and Macreadie, P. I.: The Evolution of Blue Carbon Science, Wetlands, 42, 109, https://doi.org/10.1007/s13157-022-01628-5, 2022.

Dušek, J., Nguyen, V. X., Le, T. X., and Pavelka, M.: Methane and carbon dioxide emissions from different ecosystems at the end of dry period in South Vietnam, Trop. Ecol., 62, 1–16, https://doi.org/10.1007/s42965-020-00118-1, 2021.

Epron, D., Mochidome, T., Bassar, A. T. M. Z., and Suwa, R.: Variability in methane emissions from stems and buttress roots of *Bruguiera Gymnorrhiza* trees in a subtropical mangrove forest, Ecol. Res., 1440-1703.12415, https://doi.org/10.1111/1440-1703.12415, 2023.

Evans, D. E.: Aerenchyma formation, New Phytologist, 161, 35–49, https://doi.org/10.1046/j.1469-8137.2003.00907.x, 2004.

Feng, H., Guo, J., Ma, X., Han, M., Kneeshaw, D., Sun, H., Malghani, S., Chen, H., and Wang, W.: Methane emissions may be driven by hydrogenotrophic methanogens inhabiting the stem tissues of poplar, New Phytol., 233, 182–193, https://doi.org/10.1111/nph.17778, 2022.

Gao, C.-H., Zhang, S., Ding, Q.-S., Wei, M.-Y., Li, H., Li, J., Wen, C., Gao, G.-F., Liu, Y., Zhou, J.-J., Zhang, J.-Y., You, Y.-P., and Zheng, H.-L.: Source or sink? A study on the methane flux from mangroves stems in Zhangjiang estuary, southeast coast of China, Sci. Total. Environ., 788, 147782, https://doi.org/10.1016/j.scitotenv.2021.147782, 2021.

He, Y., Guan, W., Xue, D., Liu, L., Peng, C., Liao, B., Hu, J., Zhu, Q., Yang, Y., Wang, X., Zhou, G., Wu, Z., and Chen, H.: Comparison of methane emissions among invasive and native mangrove species in Dongzhaigang, Hainan Island, Sci. Total. Environ., 697, 133945, https://doi.org/10.1016/j.scitotenv.2019.133945, 2019.

Huang, J., Jiafang Huang, Luo, M., Min Luo, Liu, Y., Yuxue, Z., and Tan, J.: Effects of Tidal Scenarios on the Methane Emission Dynamics in the Subtropical Tidal Marshes of the Min River Estuary in Southeast China., Int. J. Env. Res. Pub. He., 16, 2790, https://doi.org/10.3390/ijerph16152790, 2019.

Jackson, R. B., Saunois, M., Bousquet, P., Canadell, J. G., Poulter, B., Stavert, A. R., Bergamaschi, P., Niwa, Y., Segers, A., and Tsuruta, A.: Increasing anthropogenic methane emissions arise equally from agricultural and fossil fuel sources, Environ. Res. Lett., 15, 071002, https://doi.org/10.1088/1748-9326/ab9ed2, 2020.

Jeffrey, L. C., Reithmaier, G., Sippo, J. Z., Johnston, S. G., Tait, D. R., Harada, Y., and Maher, D. T.: Are methane emissions from mangrove stems a cryptic carbon loss pathway? Insights from a catastrophic forest mortality, New Phytol., 224, 146–154, https://doi.org/10.1111/nph.15995, 2019.

Jeffrey, L. C., Maher, D. T., Chiri, E., Leung, P. M., Nauer, P. A., Arndt, S. K., Tait, D. R., Greening, C., and Johnston, S. G.: Bark-dwelling methanotrophic bacteria decrease methane emissions from trees, Nat. Commun., 12, 2127, https://doi.org/10.1038/s41467-021-22333-7, 2021.

Jeffrey, L. C., Moras, C. A., Tait, D. R., Johnston, S. G., Call, M., Sippo, J. Z., Jeffrey, N. C., Laicher-Edwards, D., and Maher, D. T.: Large Methane Emissions From Tree Stems Complicate the Wetland Methane Budget, J. Geophys. Res. Biogeo., 128, e2023JG007679, https://doi.org/10.1029/2023JG007679, 2023.

Jeffrey, L. C., Johnston, S. G., Tait, D. R., Dittmann, J., and Maher, D. T.: Rapid bark-mediated tree stem methane transport occurs independently of the transpiration stream in Melaleuca quinquenervia, New Phytol., 242, 49–60, https://doi.org/10.1111/nph.19404, 2024.

Köhn, D., Günther, A., Schwabe, I., and Jurasinski, G.: Short-lived peaks of stem methane emissions from mature black alder (*Alnus Glutinosa* (L.) Gaertn.) – Irrelevant for ecosystem methane budgets?, Plant-Environ. Interact., 2, 16–27, https://doi.org/10.1002/pei3.10037, 2021.

Kutschera, E., Khalil, A., Rice, A., and Rosenstiel, T.: Mechanisms of methane transport through *Populus trichocarpa*, Biogeosciences, https://doi.org/10.5194/bg-2016-60, 2016.

Lee, L.-H., Hsieh, L.-Y., and Lin, H.-J.: In situ production and respiration of the benthic community during emersion on subtropical intertidal sandflats, Mar. Ecol. Prog. Ser., 441, 33–47, https://doi.org/10.3354/meps09362, 2011.

Lenhart, K., Weber, B., Elbert, W., Steinkamp, J., Clough, T., Crutzen, P., Pöschl, U., and Keppler, F.: Nitrous oxide and methane emissions from cryptogamic covers, Glob. Change Biol., 21, 3889–3900, https://doi.org/10.1111/gcb.12995, 2015.

Liao, X., Wang, Y., Malghani, S., Zhu, X., Cai, W., Qin, Z., and Wang, F.: Methane and nitrous oxide emissions and related microbial communities from mangrove stems on Qi'ao Island, Pearl River Estuary in China, Sci. Total. Environ., 915, 170062, https://doi.org/10.1016/j.scitotenv.2024.170062, 2024.

Li, S., Chen, P., Huang, J., Hsueh, M., Hsieh, L., Lee, C., and Lin, H.: Factors regulating carbon sinks in mangrove ecosystems, Glob. Change Biol., 24, 4195–4210, https://doi.org/10.1111/gcb.14322, 2018.

Li, Y., Wang, D., Chen, Z., Chen, J., Hu, H., and Wang, R.: Methane Emissions during the Tide Cycle of a Yangtze Estuary Salt Marsh, Atmosphere, 12, 245, https://doi.org/10.3390/atmos12020245, 2021.

Lin, C.-W., Kao, Y.-C., Chou, M.-C., Wu, H.-H., Ho, C.-W., and Lin, H.-J.: Methane Emissions from Subtropical and Tropical Mangrove Ecosystems in Taiwan, Forests, 11, 470, https://doi.org/10.3390/f11040470, 2020.

Lin, C.-W., Kao, Y.-C., Lin, W.-J., Ho, C.-W., and Lin, H.-J.: Effects of Pneumatophore Density on Methane Emissions in Mangroves, Forests, 12, 314, https://doi.org/10.3390/f12030314, 2021.

Lin, C.-W., Lin, W.-J., Ho, C.-W., Kao, Y.-C., Yong, Z.-J., and Lin, H.-J.: Flushing emissions of methane and carbon dioxide from mangrove soils during tidal cycles. Science of the Total Environment, 919: 170768, 2024.

Lin, W.-J., Lin, C.-W., Wu, H.-H., Kao, Y.-C., and Lin, H.-J.: Mangrove carbon budgets suggest the estimation of net production and carbon burial by quantifying litterfall, CATENA, 232, 107421, https://doi.org/10.1016/j.catena.2023.107421, 2023.

Machacova, K., Borak, L., Agyei, T., Schindler, T., Soosaar, K., Mander, Ü., and Ah-Peng, C.: Trees as net sinks for methane (CH_4) and nitrous oxide (N_2O) in the lowland tropical rain forest on volcanic Réunion Island, New Phytol., 229, 1983–1994, https://doi.org/10.1111/nph.17002, 2021.

Moldaschl, E., Kitzler, B., Machacova, K., Schindler, T., and Schindlbacher, A.: Stem CH_4 and N_2O fluxes of *Fraxinus excelsior* and *Populus alba* trees along a flooding gradient, Plant Soil, 461, 407–420, https://doi.org/10.1007/s11104-020-04818-4, 2021.

Peacock, M., Lawson, C., Gowing, D., and Gauci, V.: Water table depth and plant species determine the direction and magnitude of methane fluxes in floodplain meadow soils, Ecol. Evol., 14, e11147, https://doi.org/10.1002/ece3.11147, 2024.

Pangala, S. R., Moore, S., Hornibrook, E. R. C., and Gauci, V.: Trees are major conduits for methane egress from tropical forested wetlands, New Phytol., 197, 524–531, https://doi.org/10.1111/nph.12031, 2013.

Pangala, S. R., Gowing, D. J., Hornibrook, E. R. C., and Gauci, V.: Controls on methane emissions from *Alnus Glutinosa* saplings, New Phytol., 201, 887–896, https://doi.org/10.1111/nph.12561, 2014.

Pangala, S. R., Hornibrook, E. R. C., Gowing, D. J., and Gauci, V.: The contribution of trees to ecosystem methane emissions in a temperate forested wetland, Glob. Change Biol., 21, 2642–2654, https://doi.org/10.1111/gcb.12891, 2015.

已設定格式: 英文 (美國)

已設定格式: 字型: 非粗體

已設定格式: 字型: 非粗體

已設定格式: 字型: 非粗體

已設定格式: 字型: 非斜體

Pangala, S. R., Enrich-Prast, A., Basso, L. S., Peixoto, R. B., Bastviken, D., Hornibrook, E. R. C., Gatti, L. V., Marotta, H., Calazans, L. S. B., Sakuragui, C. M., Bastos, W. R., Malm, O., Gloor, E., Miller, J. B., and Gauci, V.: Large emissions from floodplain trees close the Amazon methane budget, Nature, 552, 230–234, https://doi.org/10.1038/nature24639, 2017.

Pitz, S. L., Megonigal, J. P., Chang, C.-H., and Szlavecz, K.: Methane fluxes from tree stems and soils along a habitat gradient, Biogeochemistry, 137, 307–320, https://doi.org/10.1007/s10533-017-0400-3, 2018.

Rosentreter, J. A., Maher, D. T., Erler, D. V., Murray, R. H., and Eyre, B. D.: Methane emissions partially offset "blue carbon" burial in mangroves, Sci. Adv., 4, eaao4985, https://doi.org/10.1126/sciadv.aao4985, 2018.

Rosentreter, J. A., Al-Haj, A. N., Fulweiler, R. W., and Williamson, P.: Methane and Nitrous Oxide Emissions Complicate Coastal Blue Carbon Assessments, Global Biogeochem. Cy., 35, e2020GB006858, https://doi.org/10.1029/2020GB006858, 2021.

Saunois, M., Stavert, A. R., Poulter, B., Bousquet, P., Canadell, J. G., Jackson, R. B., Raymond, P. A., Dlugokencky, E. J., Houweling, S., Patra, P. K., Ciais, P., Arora, V. K., Bastviken, D., Bergamaschi, P., Blake, D. R., Brailsford, G., Bruhwiler, L., Carlson, K. M., Carrol, M., Castaldi, S., Chandra, N., Crevoisier, C., Crill, P. M., Covey, K., Curry, C. L., Etiope, G., Frankenberg, C., Gedney, N., Hegglin, M. I., Höglund-Isaksson, L., Hugelius, G., Ishizawa, M., Ito, A., Janssens-Maenhout, G., Jensen, K. M., Joos, F., Kleinen, T., Krummel, P. B., Langenfelds, R. L., Laruelle, G. G., Liu, L., Machida, T., Maksyutov, S., McDonald, K. C., McNorton, J., Miller, P. A., Melton, J. R., Morino, I., Müller, J., Murguia-Flores, F., Naik, V., Niwa, Y., Noce, S., O'Doherty, S., Parker, R. J., Peng, C., Peng, S., Peters, G. P., Prigent, C., Prinn, R., Ramonet, M., Regnier, P., Riley, W. J., Rosentreter, J. A., Segers, A., Simpson, I. J., Shi, H., Smith, S. J., Steele, L. P., Thornton, B. F., Tian, H., Tohjima, Y., Tubiello, F. N., Tsuruta, A., Viovy, N., Voulgarakis, A., Weber, T. S., Van Weele, M., Van Der Werf, G. R., Weiss, R. F., Worthy, D., Wunch, D., Yin, Y., Yoshida, Y., Zhang, W., Zhang, Z., Zhao, Y., Zheng, B., Zhu, Q., Zhu, Q., and Zhuang, Q.: The Global Methane Budget 2000–2017, Earth Syst. Sci. Data, 12, 1561–1623, https://doi.org/10.5194/essd-12-1561-2020, 2020.

Schindler, T., Mander, Ü., Machacova, K., Espenberg, M., Krasnov, D., Escuer-Gatius, J., Veber, G., Pärn, J., and Soosaar, K.: Short-term flooding increases CH_4 and N_2O emissions from trees in a riparian forest soil-stem continuum, Sci. Rep., 10, 3204, https://doi.org/10.1038/s41598-020-60058-7, 2020.

Schindler, T., Machacova, K., Mander, Ü., Escuer-Gatius, J., and Soosaar, K.: Diurnal Tree Stem CH_4 and N_2O Flux Dynamics from a Riparian Alder Forest, Forests, 12, 863, https://doi.org/10.3390/f12070863, 2021.

Sjögersten, S., Siegenthaler, A., Lopez, O. R., Aplin, P., Turner, B., and Gauci, V.: Methane emissions from tree stems in neotropical peatlands, New Phytol., 225, 769–781, https://doi.org/10.1111/nph.16178, 2020.

Sturm, K., Werner, U., Grinham, A., and Yuan, Z.: Tidal variability in methane and nitrous oxide emissions along a subtropical estuarine gradient, Estuar. Coast. Shelf S., 192, 159–169, https://doi.org/10.1016/j.ecss.2017.04.027, 2017.

Takahashi, K., Sakabe, A., Azuma, W. A., Itoh, M., Imai, T., Matsumura, Y., Tateishi, M., and Kosugi, Y.: Insights into the mechanism of diurnal variations in methane emission from the stem surfaces of *Alnus Japonica*, New Phytol., 235, 1757–1766, https://doi.org/10.1111/nph.18283, 2022.

Terazawa, K., Tokida, T., Sakata, T., Yamada, K., and Ishizuka, S.: Seasonal and weather-related controls on methane emissions from the stems of mature trees in a cool-temperate forested wetland, Biogeochemistry, 156, 1–20, https://doi.org/10.1007/s10533-021-00841-4, 2021.

Terazawa, K., Yamada, K., Ohno, Y., Sakata, T., and Ishizuka, S.: Spatial and temporal variability in methane emissions from tree stems of *Fraxinus mandshurica* in a cool-temperate floodplain forest, Biogeochemistry, 123, 349–362, https://doi.org/10.1007/s10533-015-0070-y, 2015.

Teskey, R. O., Saveyn, A., Steppe, K., and McGuire, M. A.: Origin, fate and significance of CO_2 in tree stems, New Phytol., 177, 17–32, https://doi.org/10.1111/j.1469-8137.2007.02286.x, 2008.

Tong, C., Wang, W.-Q., Zeng, C.-S., and Marrs, R.: Methane (CH_4) emission from a tidal marsh in the Min River estuary, southeast China, J. Environ. Sci. Health A, 45, 506–516, https://doi.org/10.1080/10934520903542261, 2010.

Tong, C., Tong, C., Huang, J. F., Hu, Z. Q., and Jin, Y. F.: Diurnal Variations of Carbon Dioxide, Methane, and Nitrous Oxide Vertical Fluxes in a Subtropical Estuarine Marsh on Neap and Spring Tide Days, Estuaries Coasts, 36, 633–642, https://doi.org/10.1007/s12237-013-9596-1, 2013.

Vroom, R. J. E., Van Den Berg, M., Pangala, S. R., Van Der Scheer, O. E., and Sorrell, B. K.: Physiological processes affecting methane transport by wetland vegetation – A review, Aquat. Bot., 182, 103547, https://doi.org/10.1016/j.aquabot.2022.103547, 2022.

Wang, Z., Gu, Q., Deng, F., Huang, J., Megonigal, J. P., Yu, Q., Lü, X., Li, L., Chang, S., Zhang, Y., Feng, J., and Han, X.: Methane emissions from the trunks of living trees on upland soils, New Phytol., 211, 429–439, https://doi.org/10.1111/nph.13909, 2016.

Yamamoto, A., Hirota, M., Suzuki, S., Oe, Y., Zhang, P., Mariko, S., and Mariko, S.: Effects of tidal fluctuations on CO_2 and CH_4 fluxes in the littoral zone of a brackish-water lake, Limnology, 10, 229–237, https://doi.org/10.1007/s10201-009-0284-6, 2009.

Yáñez-Espinosa, L. and Angeles, G.: Does mangrove stem bark have an internal pathway for gas flow?, Trees, 36, 361–377, https://doi.org/10.1007/s00468-021-02210-y, 2022.

Zhang, C., Zhang, Y., Luo, M., Tan, J., Chen, X., Tan, F., and Huang, J.: Massive methane emission from tree stems and pneumatophores in a subtropical mangrove wetland, Plant Soil, 473, 489–505, https://doi.org/10.1007/s11104-022-05300-z, 2022.